The two Gtsf paralogs in silkworms orthogonally activate their partner PIWI proteins for target cleavage

NATSUKO IZUMI,[1,4] KEISUKE SHOJI,[1,4] TAKASHI KIUCHI,[2] SUSUMU KATSUMA,[2] and YUKIHIDE TOMARI[1,3]

[1]Laboratory of RNA Function, Institute for Quantitative Biosciences, The University of Tokyo, Bunkyo-ku, Tokyo 113-0032, Japan

[2]Department of Agricultural and Environmental Biology, Graduate School of Agricultural and Life Sciences, The University of Tokyo, Bunkyo-ku, Tokyo 113-8657, Japan

[3]Department of Computational Biology and Medical Sciences, Graduate School of Frontier Sciences, The University of Tokyo, Bunkyo-ku, Tokyo 113-0032, Japan

ABSTRACT

The PIWI-interacting RNA (piRNA) pathway is a protection mechanism against transposons in animal germ cells. Most PIWI proteins possess piRNA-guided endonuclease activity, which is critical for silencing transposons and producing new piRNAs. Gametocyte-specific factor 1 (Gtsf1), an evolutionarily conserved zinc finger protein, promotes catalysis by PIWI proteins. Many animals have multiple Gtsf1 paralogs; however, their respective roles in the piRNA pathway are not fully understood. Here, we dissected the roles of Gtsf1 and its paralog Gtsf1-like (Gtsf1L) in the silkworm piRNA pathway. We found that Gtsf1 and Gtsf1L preferentially bind the two silkworm PIWI paralogs, Siwi and BmAgo3, respectively, and facilitate the endonuclease activity of each PIWI protein. This orthogonal activation effect was further supported by specific reduction of BmAgo3-bound *Masculinizer* piRNA and Siwi-bound *Feminizer* piRNA, the unique piRNA pair required for silkworm feminization, upon depletion of Gtsf1 and Gtsf1L, respectively. Our results indicate that the two Gtsf paralogs in silkworms activate their respective PIWI partners, thereby facilitating the amplification of piRNAs.

Keywords: *Bombyx mori*; Gtsf; piRNA; PIWI

INTRODUCTION

PIWI-interacting RNAs (piRNAs) play a central role in transposon silencing in animal germ cells, thereby maintaining their genome integrity and ensuring their proper development. piRNAs are ~24–31 nt in length and guide PIWI-clade Argonaute (Ago) proteins to complementary targets, repressing their expression at the transcriptional and post-transcriptional levels (Iwasaki et al. 2015; Ozata et al. 2019). Most PIWIs possess the endonuclease activity called "slicer" and can directly cleave target RNAs (Brennecke et al. 2007; Gunawardane et al. 2007; De Fazio et al. 2011; Reuter et al. 2011). PIWI-catalyzed RNA cleavage not only silences target transposons but also produces new piRNAs (Ozata et al. 2019); target cleavage by a piRNA-guided PIWI protein (e.g., Siwi in silkworms; Aubergine [Aub] in flies) produces a long precursor of a new complementary piRNA (called pre-pre-piRNA), which is loaded into another PIWI protein (e.g., BmAgo3 in silkworms; Ago3 in flies) with its 5′ end anchored. PIWI-loaded pre-pre-piRNA is then cleaved at a downstream position by the endonuclease Zucchini (Zuc) or by another piRNA-guided PIWI protein, resulting in the production of a shorter precursor (called pre-piRNA) (Gainetdinov et al. 2018; Ozata et al. 2019; Izumi et al. 2020). The 3′ end of pre-piRNA is further shortened by the exonuclease Trimmer (PNLDC1 in mice) and methylated by the 2′-*O*-methyltransferase Hen1 (HENMT1 in mice) to generate a mature piRNA (Horwich et al. 2007; Kirino and Mourelatos 2007; Saito et al. 2007; Izumi et al. 2016; Ding et al. 2017; Zhang et al. 2017; Nishimura et al. 2018). This piRNA biogenesis pathway, which depends on reciprocal target cleavage by a pair of PIWI proteins, is called the ping-pong cycle. Since PIWI proteins cleave target RNAs at the specific position across the 10th and 11th nucleotides of the guiding piRNA, piRNA pairs produced by the ping-pong cycle show a 10-nt complementary overlap at their 5′ ends. In general, "ping" PIWI proteins (e.g., Siwi in silkworms; Aub in flies) preferentially bind piRNAs with 5′ uracil (1U), and their

[4]These authors contributed equally to this work.

Corresponding author: tomari@iqb.u-tokyo.ac.jp

Article is online at http://www.rnajournal.org/cgi/doi/10.1261/rna.079380.122.

partner "pong" PIWI proteins (e.g., BmAgo3 in silkworms; Ago3 in flies) are loaded with piRNAs bearing adenine at the 10th nucleotide (10A) through the ping-pong cycle (Brennecke et al. 2007; Gunawardane et al. 2007; Kawaoka et al. 2009; Wang et al. 2014; Nishida et al. 2015). Coupled with the ping-pong cycle, the 3′ fragment of the cleavage products by Zuc is loaded into the next PIWI protein (e.g., Siwi in silkworms; Piwi and Aub in flies) as a new pre-pre-piRNA, which is then cleaved at a downstream position again and processed into a mature piRNA. As a result, a series of "trailing" piRNAs are consecutively produced in the downstream region (Han et al. 2015; Mohn et al. 2015; Gainetdinov et al. 2018; Ozata et al. 2019). PIWI proteins and other piRNA biogenesis factors often localize to perinuclear membrane-less granules (called "nuage"), processing bodies (P-bodies), and/or mitochondrial surfaces (Iwasaki et al. 2015; Ozata et al. 2019). Some factors shuttle between different compartments during piRNA biogenesis (Ge et al. 2019), and dynamic subcellular partitioning of piRNA factors is important for the fidelity of piRNA production (Chung et al. 2021).

Gametocyte-specific factor 1 (Gtsf1), an evolutionarily conserved small zinc finger protein, has been characterized as an essential piRNA factor in mice and flies (Ipsaro and Joshua-Tor 2022). The *Drosophila* homolog of Gtsf1, Asterix, binds Piwi and functions in Piwi-mediated transcriptional silencing in the nucleus, while *asterix* mutant has no apparent effects on the piRNA biogenesis (Dönertas et al. 2013; Muerdter et al. 2013; Ohtani et al. 2013). On the other hand, mouse GTSF1 is required for the production of MIWI2-bound piRNAs, and *Gtsf1* knockout (KO) exhibits similar phenotypes as *Miwi2* KO (Yoshimura et al. 2009, 2018). In silkworms, loss of Gtsf1 causes defects in gametogenesis, sex determination, and transposon silencing accompanied by down-regulation of piRNAs (Chen et al. 2020). Recently, it was reported that mouse GTSF1 potentiates the otherwise poor endonucleolytic activity of MIWI and MILI, and that silkworm Gtsf1 has a similar activity for Siwi but not for BmAgo3 (Arif et al. 2022). Considering that sex determination in silkworms is mediated by a unique Siwi-bound piRNA called *Feminizer* (*Fem*) piRNA (Kiuchi et al. 2014), the phenotypes observed in silkworm *Gtsf1* mutant may be explained by the dysfunction of Siwi catalysis.

Many animals possess multiple Gtsf paralogs; flies have four (Gtsf1/Asterix, CG14036, CG32625, and CG34283), mice have three (GTSF1, GTSF1L, and GTSF2), and silkworms have two (Gtsf1 and Gtsf1-like [Gtsf1L]) (Supplemental Fig. 1A). However, their respective roles in the piRNA pathway are not fully understood. Here, we dissected the role of the two Gtsf paralogs in silkworms in the piRNA pathway, using a silkworm ovarian cell line called BmN4 and silkworm embryos. We found that Gtsf1 and Gtsf1L preferentially bind the two silkworm PIWI proteins, Siwi and BmAgo3, respectively, and promote the slicer activity of each PIWI protein. Their orthogonal action on the partner PIWI protein was further supported by specific reduction of *Masculinizer* (*Masc*) and *Fem* piRNAs, the ping-pong pair required for silkworm sex determination, in depletion of Gtsf1 and Gtsf1L, respectively. These results suggest that the two Gtsf paralogs in silkworms independently function in the ping-pong cycle by facilitating the slicer activity of the respective partner PIWI proteins.

RESULTS AND DISCUSSION

Gtsf1 and Gtsf1L bind and activate Siwi and BmAgo3, respectively

Silkworms have two Gtsf1 paralogs, Gtsf1 and Gtsf1-like (Gtsf1L), which have the characteristic tandem CHHC-type zinc-finger domains and show 27.8% similarity (Supplemental Fig. 1B). We have recently reported that silkworm Gtsf1 promotes the slicer activity of Siwi but not that of BmAgo3 (Arif et al. 2022). Consistent with this, physical interaction between Gtsf1 and Siwi has been demonstrated (Chen et al. 2020). On the other hand, the function of Gtsf1L remains unclear. To see if Gtsf1L binds any PIWI protein(s), we transiently expressed epitope-tagged Gtsf1 or Gtsf1L in BmN4 cells and examined the interaction with endogenous Siwi and BmAgo3. Gtsf1 was preferentially immunoprecipitated with Siwi, while Gtsf1L more specifically interacted with BmAgo3 (Fig. 1A). Although a small amount of Gtsf1 or Gtsf1L was also coimmunoprecipitated with BmAgo3 or Siwi, respectively, the canonical interactions (Siwi-Gtsf1 and BmAgo3-Gtsf1L) were more resistant to the RNase treatment than the noncanonical interactions (BmAgo3-Gtsf1 and Siwi-Gtsf1L). This orthogonal interaction was also supported by AlphaFold-Multimer (Supplemental Fig. 1C,D), and the carboxy-terminal structure of Gtsf1 and Gtsf1L was predicted with higher reliability when complexed with Siwi and BmAgo3, respectively (Supplemental Fig. 1E,F). In contrast, interactions between Gtsf proteins and AGO-clade Argonaute proteins, BmAgo1 and BmAgo2, were not predicted by AlphaFold-Multimer (Supplemental Fig. 1C,D). As with mouse GTSF1, which directly interacts with TDRD9 [Spindle-E (SpnE) ortholog in mice] (Yoshimura et al. 2018), SpnE was also preferentially coimmunoprecipitated with Gtsf1 (Fig. 1A; Supplemental Fig. 1G).

Considering this different binding preference, we reexamined the effect of recombinant Gtsf proteins on the slicer activity of Siwi or BmAgo3 in vitro. We first prepared a target RNA complementary to an endogenous Siwi-bound piRNA and monitored target cleavage by Siwi immunoprecipitates in the presence or absence of recombinant Gtsf1 or Gtsf1L (Fig. 1B; Supplemental Fig. 1H). As previously reported (Arif et al. 2022), we confirmed that Gtsf1 but not Gtsf1L promotes target cleavage by Siwi (Fig. 1B). In the previous study, the target cleavage activity by BmAgo3 was extremely inefficient, making it difficult to conclusively

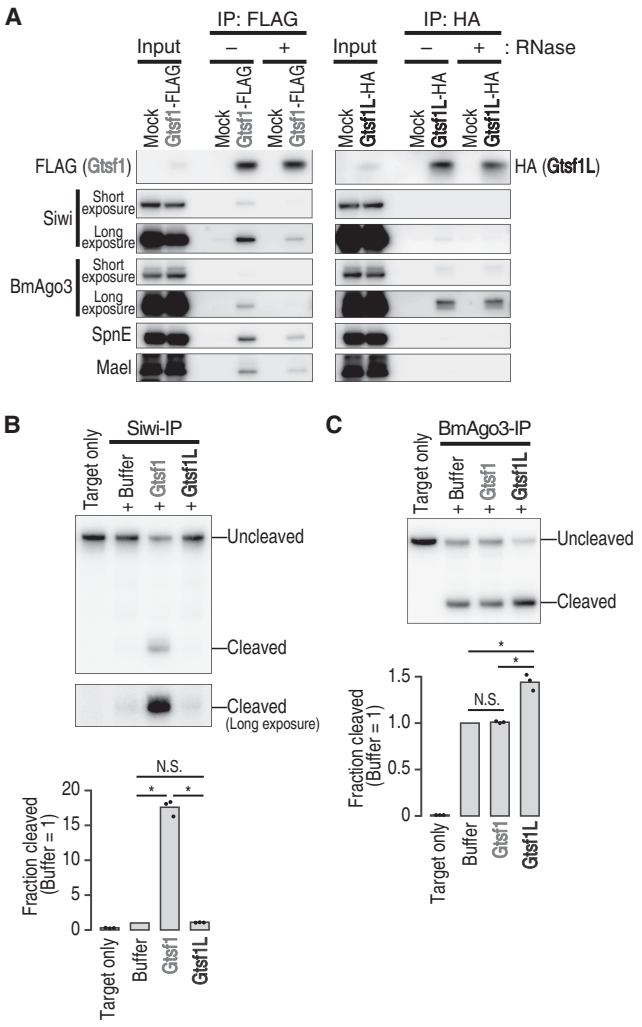

FIGURE 1. Gtsf1 and Gtsf1L bind Siwi and BmAgo3, respectively, and activate each PIWI protein. (*A*) Western blot analysis of immunoprecipitated tagged-Gtsf1 and -Gtsf1L from BmN4 cells. After immunoprecipitation, the sample was divided into two and one half was treated with RNase A. (*B*,*C*) In vitro target cleavage assay of immunoprecipitated Siwi (*B*) or BmAgo3 (*C*) from BmN4 cells. Target RNA against an abundant endogenous Siwi- (*B*) or BmAgo3-bound (*C*) piRNA was used. The graphs show the fraction cleaved normalized to that of the buffer-only sample. The values are means of three independent experiments. Dots, individual values. Paired *t*-test with Bonferroni adjusted *P*-values are 0.0046 (Buffer vs. Gtsf1 in *B*), 0.0049 (Gtsf1 vs. Gtsf1L in *B*), 0.04 (Buffer vs. Gtsf1L in *C*), and 0.039 (Gtsf1 vs. Gtsf1L in *C*). N.S., not significant.

examine the activity of Gtsf1L (Arif et al. 2022). We therefore searched for a better target sequence for an endogenous BmAgo3-bound piRNA. By using this new target, we could detect modest but significant enhancement of BmAgo3-mediated target cleavage by Gtsf1L but not by Gtsf1 (Fig. 1C). Taken together, these data suggest that Gtsf1 and Gtsf1L specifically interact with Siwi and BmAgo3, respectively, and facilitate the slicer activity of each PIWI protein.

Gtsf1 and Gtsf1L accumulate in the complex of catalytically inactive Siwi and BmAgo3, respectively

Because both Gtsf1 and Gtsf1L are expected to function in the catalytic process of PIWI proteins (Fig. 1B,C; Arif et al. 2022), we next examined their interaction with PIWI catalytic mutants. We coexpressed epitope-tagged Gtsf1 and wild-type (WT) or catalytically inactive (D670A) Siwi in BmN4 cells, and immunoprecipitated Gtsf1. Compared to Siwi-WT, Siwi-D670A showed markedly increased association with Gtsf1 (Fig. 2A). Although Gtsf1 was broadly distributed in the nucleus and cytoplasm with little colocalization with Siwi-WT, Gtsf1 showed partial but clear colocalization with Siwi-D670A granules (Fig. 2B), suggesting that Siwi-D670A traps Gtsf1. We previously reported that Siwi-D670A localizes to P-bodies with SpnE (Chung et al. 2021). In addition, in mouse gonocytes, GTSF1 localizes to piP-bodies (Yoshimura et al. 2018), which share components with P-bodies, together with MIWI2, TDRD9 (SpnE ortholog in mice) and MAEL (Aravin et al. 2009). Since Gtsf1 interacts with SpnE and Mael (Fig. 1A), we expected that Gtsf1 trapped by Siwi-D670A is localized to P-bodies. Indeed, we observed granular colocalization among Siwi-D670A, Gtsf1, and Dcp2, a P-body marker (Fig. 2C). In contrast, colocalization between Gtsf1 and Dcp2 was not detected when Siwi-WT was expressed (Fig. 2C). Thus, Gtsf1 is not a stable resident of P-bodies but can be trapped in P-bodies by catalytically inactive Siwi.

We next investigated the association between Gtsf1L and the catalytic mutant of BmAgo3 (D697A). We coexpressed epitope-tagged BmAgo3-WT or -D697A and Gtsf1L in BmN4 cells, and immunoprecipitated BmAgo3. The steady-state level of Gtsf1L was greatly increased by the coexpression of BmAgo3-D697A (Fig. 2D, input). Correspondingly, coimmunoprecipitation of Gtsf1L with BmAgo3-D697A was markedly higher than that with BmAgo3-WT (Fig. 2D). Unlike Gtsf1, Gtsf1L was well colocalized with BmAgo3 granules regardless of the catalytic activity of BmAgo3 (Fig. 2E). The catalytic mutation of BmAgo3 slightly intensified the BmAgo3-Gtsf1L granules, and also increased the granule formation of Siwi, a part of which partially overlapped with BmAgo3 and Gtsf1L (Fig. 2E, BmAgo3-D697A).

We next examined the behavior of Gtsf1L in *Siwi* knockdown (KD), where the handover of RNAs from BmAgo3 to Siwi in the ping-pong cycle is inhibited (Nishida et al. 2020), thereby creating an analogous situation as the catalytic inactivation of BmAgo3. Similar to the overexpression of BmAgo3-D697A, *Siwi*-KD increased the steady-state abundance of Gtsf1L and its association with BmAgo3 (Supplemental Fig. 2A). Given that *Siwi*-KD is reported to cause accumulation of BmAgo3-mediated cleavage fragments in the BmAgo3 complex (Nishida et al.

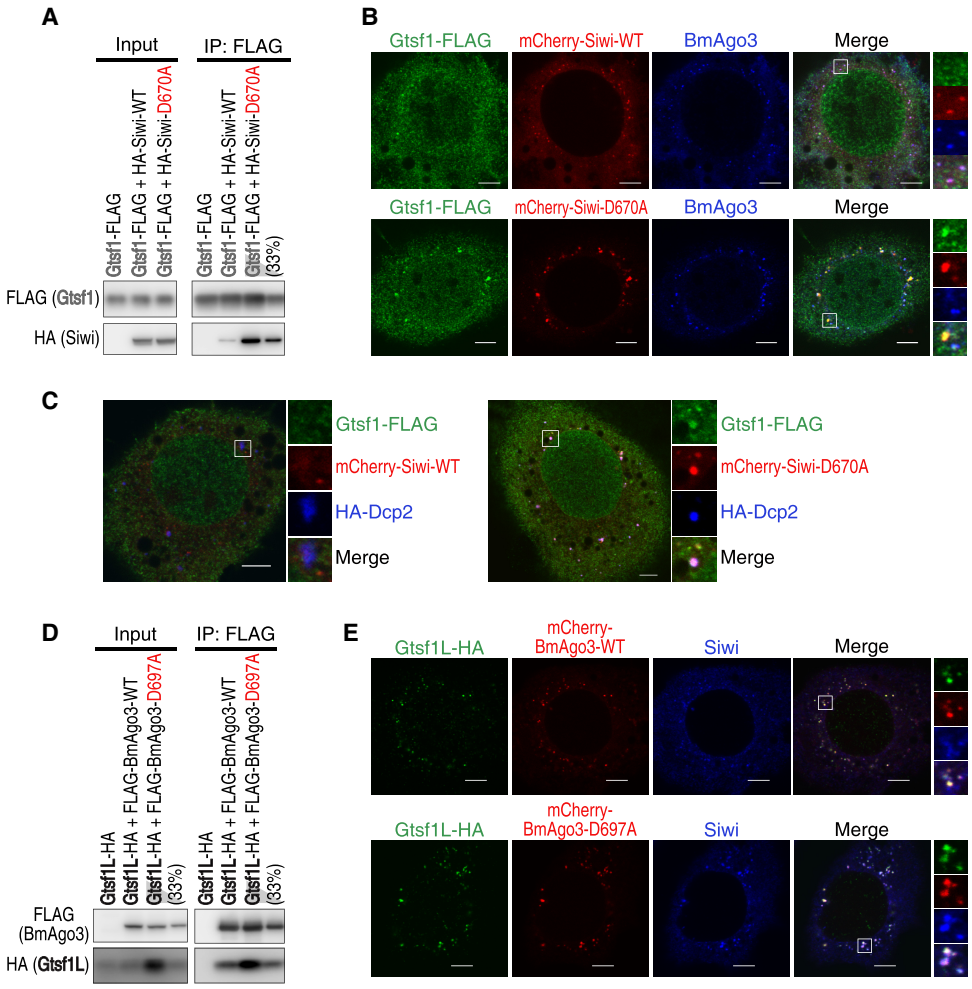

FIGURE 2. Gtsf1 and Gtsf1L show increased association with catalytically inactive Siwi and BmAgo3, respectively. (*A*) Western blot analysis of the interaction between Gtsf1-FLAG and HA-tagged wild-type (WT) Siwi or catalytically inactive Siwi-D670A. (*B*) Subcellular localization of Gtsf1-FLAG coexpressed with mCherry-Siwi or -Siwi-D670A. Scale bar, 5 µm. (*C*) Subcellular localization of Gtsf1-FLAG coexpressed with mCherry-Siwi or -Siwi-D670A, and HA-Dcp2, a P-body marker. Scale bar, 5 µm. (*D*) Western blot analysis of the interaction between Gtsf1L-HA and FLAG-tagged wild-type (WT) BmAgo3 or catalytically inactive BmAgo3-D697A. (*E*) Subcellular localization of Gtsf1L-HA coexpressed with mCherry-BmAgo3 or -BmAgo3-D697A. Scale bar, 5 µm.

2020), Gtsf1L may stay bound to BmAgo3 after the target cleavage until the cleavage fragments are handed over to Siwi. In agreement with the increased association, Gtsf1L strongly accumulated in the enlarged BmAgo3 granules in *Siwi*-KD (Supplemental Fig. 2B). In contrast to Gtsf1L, neither the Gtsf1-Siwi interaction nor their colocalization was changed by *BmAgo3*-KD (Supplemental Fig. 2C,D). The different behavior of Gtsf1 and Gtsf1L in *BmAgo3*-KD or *Siwi*-KD may reflect the fact that Siwi, but not BmAgo3, can operate homotypic ping-pong, especially in the absence of the counterpart PIWI protein (N Izumi, K Shoji, T Kiuchi, S Katsuma, and Y Tomari, unpubl.) similarly to Aub:Aub homotypic ping-pong in *ago3* mutant flies (Li et al. 2009a). In sum, our observations that Gtsf1 and Gtsf1L accumulate in the complex of their catalytically inactive PIWI partner underscore their roles in the PIWI catalytic process.

Loss of Gtsf1 and Gtsf1L reduces *Masc* and *Fem* piRNAs, respectively

In silkworms, the ping-pong cycle normally operates between Siwi and BmAgo3 (Kawaoka et al. 2009; Nishida et al. 2015). If Gtsf1 and Gtsf1L promote the slicer activity of Siwi and BmAgo3, respectively, loss of Gtsf1 and Gtsf1L should differently affect Siwi- and BmAgo3-bound piRNAs. We therefore sequenced small RNAs from BmN4 cells treated with dsRNA for *Gtsf1* or *Gtsf1L*. Either knockdown modestly decreased total mature piRNAs and the strength of the ping-pong signature, suggesting the impairment of the ping-pong cycle (Supplemental Fig. 3A,B). Because Siwi- and BmAgo3-bound piRNAs have the 1U and 10A bias, respectively (Kawaoka et al. 2009; Nishida et al. 2015), we next examined the change in 1U (but not 10A) and 10A (but not

1U) piRNAs. *Gtsf1*-KD modestly decreased both 1U- and 10A-piRNAs, while *Gtsf1L*-KD caused more severe reduction of 1U-piRNAs than 10A-piRNAs (Fig. 3A,B). The ping-pong piRNAs are generally mapped densely in discrete genomic loci and their production can be heavily influenced by neighboring piRNAs; the 3′ end processing of a piRNA is often mediated by another piRNA-guided cleavage in the downstream region (Hayashi et al. 2016; Izumi et al. 2020). Therefore, we focused on an isolated, well-defined ping-pong pair, *Fem* and *Masc* piRNAs, which determine femaleness in silkworms (Fig. 3C). *Fem* piRNA, deriving from the W chromosome, is exclusively loaded into Siwi and cleaves *Masc* mRNA, leading to the reduction of Masc protein and the suppression of masculinization (Kiuchi et al. 2014). *Fem* piRNA-mediated cleavage of *Masc* mRNA produces BmAgo3-bound *Masc* piRNA, which in turn cleaves *Fem* RNA and amplifies *Fem* piRNA via the ping-pong cycle (Kiuchi et al. 2014). No other evident ping-pong pair is found on *Fem* RNA and *Masc* mRNA, thus the effect from neighboring piRNAs can be ignored. Strikingly, *Gtsf1*-KD and *Gtsf1L*-KD specifically decreased *Masc* piRNA and *Fem* piRNA, respectively (Fig. 3C). This data supports the idea that Gtsf1 activates Siwi to promote the production of BmAgo3-bound *Masc* piRNA, while Gtsf1L activates BmAgo3 to promote the production of Siwi-bound *Fem* piRNA. Considering that both *Fem* and *Masc* piRNAs are reduced in Gtsf1 knockout (KO) silkworms (Chen et al. 2020), our transient knockdown method is probably more suitable to observe the direct (first-round) effect of the two Gtsf proteins on the piRNA biogenesis.

Gtsf1 and Gtsf1L independently function in the ping-pong cycle in vivo

In the early embryonic stages of silkworms, maternally inherited piRNAs initiate acute and massive amplification of new piRNAs via the ping-pong cycle (Kawaoka et al. 2011). In this regard, silkworm embryos may be better suited to monitor the effect of Gtsf proteins in the ping-pong cycle, compared to the cell line BmN4, where piRNAs are constantly

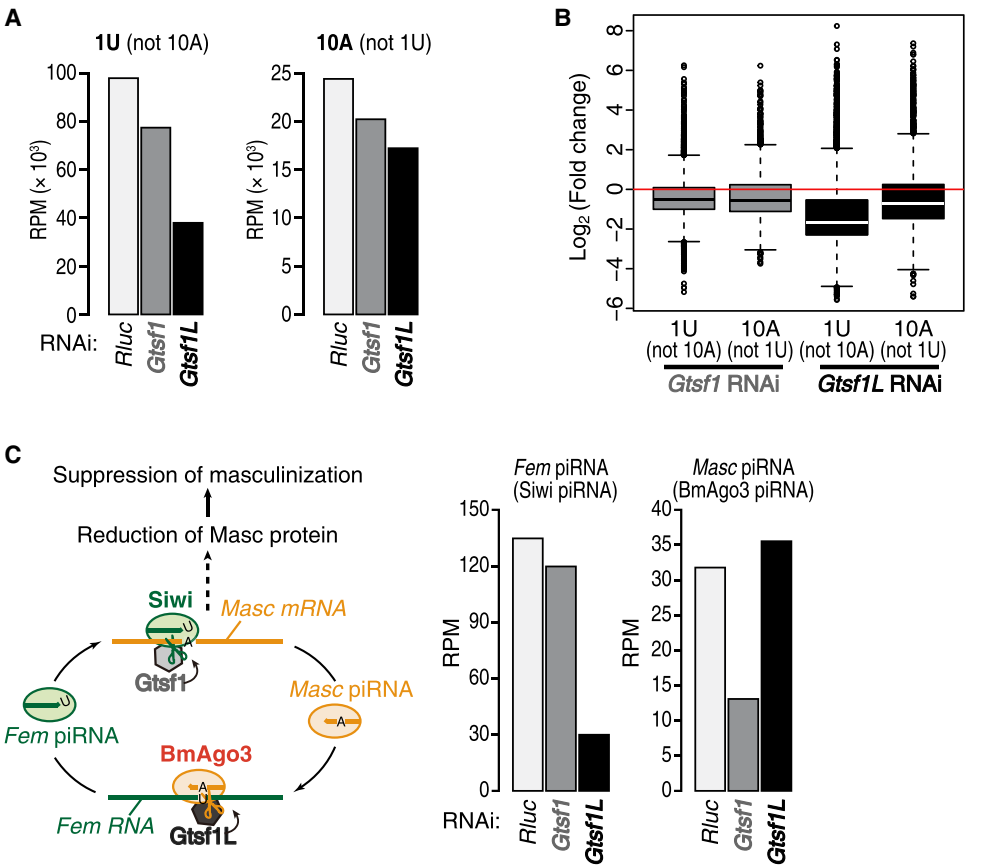

FIGURE 3. Knockdown of *Gtsf1* and *Gtsf1L* decreases *Masc* and *Fem* piRNAs, respectively. (*A*) Normalized reads of 1U (but not 10A) or 10A (but not 1U) small RNA from BmN4 cells transfected with dsRNA for *Renilla luciferase* (*Rluc*, control), *Gtsf1* or *Gtsf1L*. (*B*) Box plots showing the expression change of 1U (but not 10A) and 10A (but not 1U) piRNAs by knockdown of *Gtsf1* or *Gtsf1L* relative to control knockdown in BmN4 cells. Center line, median; box limits, upper and lower quartiles; whiskers, 1.5 × interquartile range; points, outliers. (*C*) Schematic representation of the production of *Fem* and *Masc* piRNAs via the ping-pong cycle (*left*). The expression of *Fem* and *Masc* piRNAs in *Gtsf1*- or *Gtsf1L*-knockdown (*right*).

produced and influencing each other in a steady state. To see if Gtsf1 and Gtsf1L function in a PIWI-type specific manner in vivo, we injected siRNAs against *Gtsf1* or *Gtsf1L* into silkworm embryos (Supplemental Fig. 4A) and examined piRNA production after 120 h post-injection. We prepared small RNA libraries from the embryos with two biological replicates per each knockdown condition. Consistent with the result in BmN4 cells, *Gtsf1*-KD and *Gtsf1L*-KD reduced the strength of the ping-pong signature (Supplemental Fig. 4B). Moreover, *Masc* and *Fem* piRNA were specifically decreased by *Gtsf1*-KD and *Gtsf1L*-KD, respectively (Fig. 4A), confirming the orthogonal functions of the

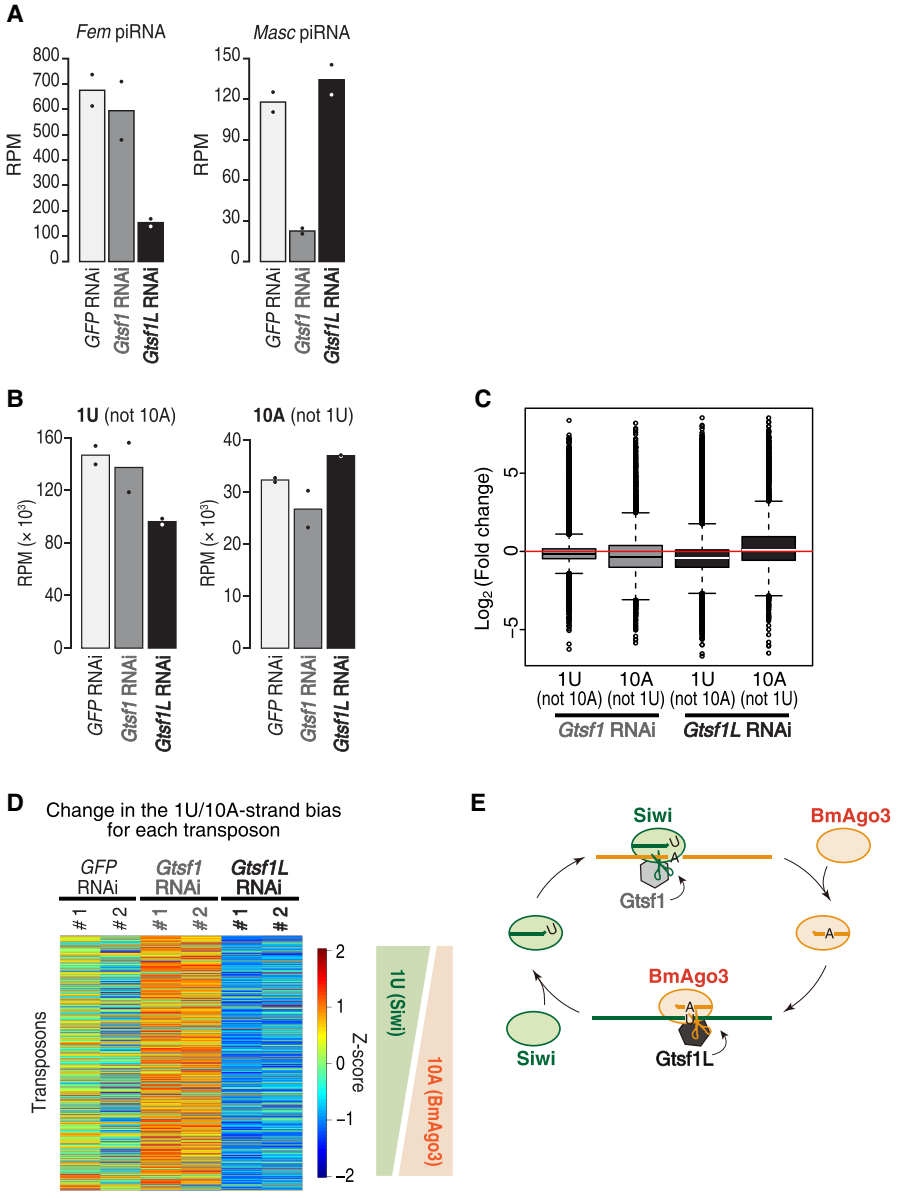

FIGURE 4. Gtsf1 and Gtsf1L separately function in the ping-pong cycle in vivo. (*A*) The expression of *Fem* and *Masc* piRNAs in silkworm embryos injected with siRNAs for *GFP* (control), *Gtsf1* or *Gtsf1L*. The values are means of two biological replicates. Dots, individual values. (*B*) Normalized reads of 1U (but not 10A) or 10A (but not 1U) small RNA from silkworm embryos injected with siRNAs for *GFP* (control), *Gtsf1* or *Gtsf1L*. The values are means of two biological replicates. Dots, individual values. (*C*) Box plots showing the expression change of 1U (but not 10A) and 10A (but not 1U) piRNAs by knockdown of *Gtsf1*or *Gtsf1L* relative to *GFP* (control) knockdown in embryos. Center line, median; box limits, upper and lower quartiles; whiskers, 1.5 × interquartile range; points, outliers. (*D*) Heatmap representation of relative changes in the 1U/10A strand bias between six samples for each transposon. The 1U/10A strand bias tends to increase (i.e., relative reduction of 10A-biased BmAgo3 piRNA) and decrease (i.e., relative reduction of 1U-biased Siwi piRNA) in *Gtsf1*- and *Gtsf1L*-knockdown, respectively. Two biological replicates per each knockdown condition. (*E*) A model for the role of two silkworm Gtsf proteins in the ping-pong cycle. Gtsf1 and Gtsf1L contribute to the production of BmAgo3- and Siwi-piRNAs by facilitating target cleavage of Siwi and BmAgo3, respectively.

two Gtsf paralogs in vivo. We also observed that, in general, 1U (but not 10A) piRNAs are down-regulated by *Gtsf1L*-KD, whereas 10A (but not 1U) piRNAs are decreased by *Gtsf1*-KD (Fig. 4B,C). In silkworms, each transposon shows different strand bias of 1U piRNAs (predominantly Siwi-piRNAs) and 10A piRNAs (predominantly BmAgo3-piRNAs) (Kawaoka et al. 2009). Therefore, we focused on 775 transposons in which 1U (but not 10A) piRNAs are disproportionally enriched on either of the two strands ("1U strand") while 10A (but not 1U) piRNAs are reciprocally enriched on the other strand ("10A strand"). We then calculated the ratio of mapped piRNA reads on the 1U and 10A strands ("1U/10A strand bias") for each transposon and monitored the change of the bias (Z-score) upon *Gtsf1*-KD or *Gtsf1L*-KD (Fig. 4D). We found that, for nearly all the transposons analyzed, *Gtsf1*-KD increased the 1U/10A strand bias (i.e., 10A [but not 1U] piRNAs were more reduced than 1U [but not 10A] piRNAs), while *Gtsf1L*-KD decreased the 1U/10A strand bias (i.e., 1U [but not 10A] piRNAs were more down-regulated). These results strengthen the idea that Gtsf1 and Gtsf1L orthogonally activate the target cleavage by Siwi and BmAgo3, thereby promoting the production of BmAgo3-bound and Siwi-bound piRNAs, respectively, in vivo.

In this study, we revealed that the two Gtsf paralogs in silkworms, Gtsf1 and Gtsf1L, individually function in the ping-pong cycle by promoting the slicer activity of Siwi and BmAgo3, respectively (Fig. 4E). In mice, GTSF1 accelerates the target cleavage by MILI and MIWI, while the other two GTSF paralogs, GTSF1L and GTSF2, can potentiate the catalytic activity of MIWI, at least in vitro (Arif et al. 2022). However, double knockout mice of *Gtsf1l* and *Gtsf2* exhibit no defects in spermatogenesis and retrotransposon silencing (Takemoto et al. 2016), suggesting that GTSF1 alone is shared by MIWI and MILI for their catalytic activation in mice. On the other hand, we found that the two Gtsf proteins in silkworms have specific preferences for the two PIWI proteins, respectively, and cannot compensate for each other. Thus, silkworm Gtsf proteins have evolved to specialize for each PIWI protein. Both Gtsf1 and Gtsf1L orthologs are found in lepidoptera and mosquitos, therefore their separate roles in the ping-pong cycle may be widely conserved in these insects. Sequence comparison of Gtsf homologs in multiple species has suggested that the diversity in their carboxy-terminal unstructured region is involved in the PIWI specificity (Arif et al. 2022). In agreement with this hypothesis, the carboxy-terminal structures of Gtsf1 and Gtsf1L were predicted with higher confidence when complexed with Siwi and BmAgo3, respectively, by AlphaFold-Multimer (Supplemental Fig. 1E). Considering that the steady state abundance of Gtsf1L is markedly increased by coexpression of catalytically inactive BmAgo3 (Fig. 2D), binding to BmAgo3 may stabilize the Gtsf1L protein itself.

How do Gtsf proteins accelerate target cleavage by PIWI? A recent structural study in *Ephydatia fluviatilis* PIWI revealed that after recognition of target RNA, extensive base pairing between piRNA and target RNA induces a conformational change in PIWI (Anzelon et al. 2021). Accordingly, it has been proposed that such a catalytic competent state of PIWI is stabilized by Gtsf1 (Arif et al. 2022). Indeed, AlphaFold-Multimer predicts that both Gtsf proteins locate around the catalytic PIWI domain (Supplemental Fig. 1F). Moreover, the first zinc finger motif of mouse GTSF1, which has RNA binding activity, is required to promote PIWI slicing (Ipsaro et al. 2021; Arif et al. 2022). Therefore, it is likely that Gtsf binds to the PIWI domain and the target RNA simultaneously to stabilize the catalytic competent conformation of PIWI proteins. The observation that both silkworm Gtsf1 and Gtsf1L accumulate in the catalytically inactive PIWI complex also supports the idea that Gtsf proteins have a higher affinity to the target-bound state of PIWI proteins. Future structural analysis of the Gtsf-PIWI complex is awaited to understand how Gtsf binding contributes to the structural change of PIWIs during the target cleavage.

MATERIALS AND METHODS

Cell culture, plasmid transfection, and dsRNA transfection in BmN4 cells

BmN4 cells were cultured at 27°C in IPL-41 medium (AppliChem) supplemented with 10% fetal bovine serum. For immunoprecipitation experiments, a total of 5–7.5 µg of plasmid and dsRNAs were transfected into BmN4 cells (2–2.5 × 10^6 cells per 10 cm dish) with X-tremeGENE HP DNA Transfection Reagent (Sigma), and the transfected cells were harvested after 4 d. For cotransfection experiments, the second transfection was performed 2 d after the first transfection, and the cells were harvested after an additional 4 d. For immunofluorescence experiments, a total of 0.4 µg of plasmid and dsRNAs were transfected into BmN4 cells (4–6 × 10^4 cells per glass bottom 35 mm dish) with X-tremeGENE HP DNA Transfection Reagent (Sigma), and cells were fixed 4 d later. For Supplemental Figure 2, transfection was repeated 2 d later and cells were fixed 4 d after the second transfection. For library preparation, 5 µg of dsRNAs were transfected into BmN4 cells (8 × 10^5 cells per 10 cm dish) with X-tremeGENE HP DNA Transfection Reagent (Sigma) every 3 d four times. dsRNA preparation was described previously (Izumi et al. 2020). Template DNAs were prepared by PCR using primers containing T7 promoter listed in Supplemental Table 1.

Plasmid construction

pIZ-FLAG-BmAgo3, pIZ-mCherry-Siwi, pIZ-mCherry-Siwi-D670A, pIZ-mCherry-BmAgo3, and pIZ-mCherry-BmAgo3-D697A were described previously (Kawaoka et al. 2009; Chung et al. 2021). The primer sequences for plasmid construction are listed in Supplemental Table 1.

pIExZ-Gtsf1-FLAG

cDNA fragment of Gtsf1 was amplified by RT-PCR from BmN4 total RNAs and cloned into pIExZ vector (Izumi et al. 2020) by an In-Fusion Cloning Kit (Takara).

pIZ-Gtsf1L-HA

A cDNA fragment of Gtsf1L was amplified by RT-PCR from BmN4 total RNAs and cloned into pIZ vector by an In-Fusion Cloning Kit (Takara).

pIZ-HA-Siwi, Siwi-D670A, pIZ-FLAG-BmAgo3-D697A

A DNA fragment coding HA-tagged Siwi was amplified by PCR and cloned into pIZ vector (Thermo Fisher/Invitrogen) by an In-Fusion Cloning Kit (Takara). pIZ-Siwi-D670A and pIZ-BmAgo3-D697A mutants were generated by site-directed mutagenesis.

pIExZ-HA-Dcp2

A DNA fragment coding HA-tagged Dcp2 was amplified by PCR and cloned into pIExZ vector (Izumi et al. 2020) by an In-Fusion Cloning Kit (Takara).

pCold-Gtsf1-7His, pCold-Gtsf1L-6His

A DNA fragment coding carboxy-terminally His-tagged Gtsf1 or Gtsf1L was amplified by PCR and cloned into pCold vector (Takara) by an In-Fusion Cloning Kit (Takara). For Gtsf1L, the coding sequence was codon-optimized to *Bombyx mori* using EMBOSS Backtranseq (http://www.ebi.ac.uk/Tools/st/emboss_backtranseq/), and a synthesized DNA fragment (GenScript) was used as PCR template.

Antibodies and western blotting

Rabbit anti-Siwi, anti-BmAgo3, and anti-Mael antibodies were described previously (Chung et al. 2021; Izumi et al. 2020). Rabbit anti-SpnE antibody was generated by immunizing amino-terminally His-tagged recombinant SpnE (aa 2–124). Anti-FLAG (M2, Sigma), anti-HA (3F10, Roche), anti-α-Tubulin (B-5-1-2, Sigma) antibodies were purchased. For Supplemental Figure 2, the anti-BmAgo3 antibody was biotinylated using the Biotin Labeling Kit-NH_2 (DOJINDO). Chemiluminescence was induced by Luminata Forte Western HRP Substrate (Millipore) and images were acquired by Amersham Imager 600 (GE Healthcare).

Immunoprecipitation

BmN4 cells were resuspended in buffer A [25 mM Tris-HCl (pH 7.4), 150 mM NaCl, 1.5 mM $MgCl_2$, 0.15% Triton X-100, 0.5 mM DTT, 1× Complete EDTA-free protease inhibitor (Roche), 1× PhosSTOP (Roche)] and incubated on ice for 20 min. The cell suspension was centrifuged at 17,000*g* for 30 min at 4°C. The supernatant was incubated with Dynabeads Protein G (Thermo Fisher/Invitrogen) preconjugated with anti-FLAG antibody (M2, Sigma). For HA-immunoprecipitation, the supernatant was preincubated with anti-HA antibody (3F10, Sigma) at 4°C for 30 min, and then Dynabeads Protein G (Thermo Fisher/Invitrogen) was added. After incubation at 4°C for 1 h, the immunoprecipitated beads were divided into two and incubated in buffer A with/without 200 µg/mL RNase A (Qiagen) at 30°C for 15 min. The beads were washed with buffer B [25 mM Tris-HCl (pH 7.4), 150 mM NaCl, 1.5 mM $MgCl_2$, 0.5% Triton X-100, 0.5 mM DTT] five times, and the immunopurified complexes were eluted with 3× FLAG peptide (Sigma) or HA peptide (MBL).

Purification of recombinant proteins

pCold-Gtsf1-7His or Gtsf1L-6His was transformed into Rosetta 2 (DE3) competent cells (Novagen). The cells were cultured at 37°C until the OD_{600} reaches ~0.6, and then cooled on ice for 30 min. Protein expression was induced with 1 mM IPTG at 15°C for 15 h. The cell pellets were resuspended in TALON lysis buffer [50 mM Hepes-KOH (pH 7.4), 300 mM NaCl, 15 mM imidazole, 0.2 mM TECP, 10 µg/mL leupeptin, 10 µg/mL aprotinin, 1 µg/mL pepstatin A, 1× EDTA-free protease inhibitor cocktail (Roche)] and sonicated with Bioruptor II (CosmoBio). The cell lysate was centrifuged at 17,000*g* at 4°C for 20 min. The cleared lysate was added to TALON CellThru Resin (Takara) and incubated at 4°C for 1 h. After washing the resin with TALON lysis buffer, the bound proteins were eluted with elution buffer [50 mM Hepes-KOH (pH 7.4), 150 mM NaCl, 300 mM imidazole, 0.2 mM TECP]. Peak fractions were pooled and dialyzed with PBS overnight.

In vitro cleavage assay

For Siwi and BmAgo3 immunoprecipitation, BmN4 cells were resuspended in buffer C [25 mM Tris-HCl (pH 7.4), 150 mM NaCl, 1.5 mM $MgCl_2$, 1% Triton X-100, 0.5 mM DTT, 1× Complete EDTA-free protease inhibitor (Roche), 1× PhosSTOP (Roche)] and incubated on ice for 20 min. The cell suspension was centrifuged at 17,000*g* for 30 min at 4°C. The supernatant was preincubated with anti-Siwi or anti-BmAgo3 antibody at 4°C for 1 h, and then Dynabeads Protein G (Thermo Fisher/Invitrogen) was added. The mixture was further incubated at 4°C overnight. The beads were washed with buffer C five times, rinsed with buffer D [30 mM Hepes-KOH (pH 7.4), 100 mM KOAc, 2 mM $Mg(OAc)_2$, 0.5 mM DTT], and divided for different target cleavage conditions. Target cleavage assay was performed at 28°C for 2 h in a 10 µL reaction containing 3 µL of 40× reaction mix (Haley et al. 2003), 100 nM recombinant proteins and 1 nM ^{32}P cap-radiolabeled target RNA. The target RNA was purified by EtOH precipitation following proteinase K treatment and run on 8% denaturing polyacrylamide gel. The images were acquired with the FLA-7000 imaging system (Fujifilm Life Sciences) and quantified using ImageJ/Fiji. The target RNA against an abundant endogenous Siwi or BmAgo3 piRNA was prepared by in vitro transcription as described previously (Yoda et al. 2010). Primers used for target RNA preparation were described in Supplemental Table 1.

RNAi in silkworm embryos

siRNA-mediated embryonic knockdown was performed as previously described (Kiuchi et al. 2014; Kiuchi and Katsuma 2022). In brief, ~5 nL of 100 µM siRNA (FASMAC) was injected into a *Bombyx mori* N4 strain embryo within 3 h after oviposition using IM 300 Microinjector (Narishige). The embryos were incubated at 25°C in a humidified petri dish for 120 h. Approximately 12 embryos were collected as one sample and total RNA was extracted. siRNA sequences are listed in Supplemental Table 1.

RNA extraction and quantitative real-time PCR

Total RNAs prepared by TRI Reagent (Molecular Research Center) were used for real-time PCR and preparation of small RNA libraries. Five hundred nanograms of total RNA was reverse transcribed by a PrimeScript RT Reagent Kit with gDNA Eraser (Takara), and qRT-PCR was performed using KAPA SYBR FAST Master Mix (2×) Universal (Kapa Biosystems) and the Thermal Cycler Dice Real Time System (Takara). The primer sequences for real-time PCR are listed in Supplemental Table 1.

Immunofluorescence

BmN4 cells were fixed with 4% paraformaldehyde in PBS at room temperature for 10 min, then the cells were permeabilized with 0.3% Triton X-100 in PBS for 5 min. After preincubation with blocking buffer [PBS supplemented with 1% BSA (Sigma) and 0.1% Triton X-100] at room temperature for 1 h, the cells were incubated with primary antibodies [anti-FLAG antibody (M2, Sigma, 1/250), anti-HA antibody (3F10, Roche, 1/300), anti-Siwi antibody (1/400), anti-BmAgo3 antibody (1/250)] in blocking buffer at 4°C overnight. Alexa Fluor 488 donkey anti-mouse IgG, Alexa Fluor 488 donkey anti-rat IgG, Alexa Fluor 647 donkey anti-rabbit IgG, and Alexa Fluor 647 goat anti-rat IgG secondary antibodies (Thermo Fisher/Invitrogen) were used for detection. For Supplemental Figure 2, BmAgo3 was probed with biotinylated anti-BmAgo3 antibody after incubation with the secondary antibody, and the BmAgo3 signal was detected by Cy3-Streptavidin (Jackson ImmunoResearch). Images were captured using the Olympus FV3000 confocal laser scanning system with a 60× oil immersion objective lens (PLAPON 60XO, NA 1.42, Olympus) and processed FV31S-SW Viewer software and Adobe Photoshop Elements 10.

Small RNA library preparation

Small RNA libraries were constructed from 20–50 nt total RNAs according to the Zamore lab's open protocol (https://www.dropbox.com/s/r5d7aj3hhyaborq/) with some modifications (Fu et al. 2018). Ten synthetic 22-nt oligoribonucleotides (GeneDesign) (Williams et al. 2013) were spiked in all samples for normalization. The 3′ adapter was conjugated with an amino CA linker instead of dCC at the 3′ end (GeneDesign) and adenylated using a 5′ DNA adenylation kit at the 5′ end (NEB). To reduce a ligation bias, four random nucleotides were included in the 3′ and 5′ adapters [(5′-rAppNNNNTGGAATTCTCGGGTGCCAAGG/amino CA linker-3′) and (5′-GUUCAGAGUUCUACAGUCCGACGAUCNNNN-3′)] and the adapter ligation was performed in the presence of 20% PEG-8000. After the 3′ adapter ligation at 16°C for ≥16 h, RNAs were size-selected by urea PAGE. For RNA extraction from a polyacrylamide gel, ZR small-RNA PAGE Recovery Kit (ZYMO Research) was used. Small RNA libraries were sequenced using the Illumina HiSeq 4000 platform to obtain 50-nt single-end reads.

Sequence analysis of small RNA library

After removal of the adaptor sequences by cutadapt (Martin 2011), 20–45 nt reads without any ambiguous bases were used for the following analyses. These piRNA libraries were normalized by the read count of spikes.

Definition of 1U and 10A piRNAs

The RPM of each piRNA was calculated based on an assumption that if 1–26 nt sequences were identical, they were the same piRNA. For piRNA analysis of BmN4 cells and embryos, only highly expressed piRNAs (RPM > 1) in any of the three BmN4 libraries and six embryo libraries were extracted and used. The common parts (1–26 nt) of these piRNAs were mapped to transposons allowing two mismatches with Bowtie (Osanai-Futahashi et al. 2008; Langmead et al. 2009). The mapped piRNAs, including 16,734 species of 1U (but not 10A) piRNAs and 6869 species of 10A (but not 1U) piRNAs for BmN4 cell libraries, and 22,374 species of 1U (but not 10A) piRNAs and 8533 species of 10A (but not 1U) piRNAs for embryo libraries, were extracted and used. Sam files were converted to bam files by SAMtools (Li et al. 2009b) and then to bed files by BEDTools (Quinlan and Hall 2010). The length and 5′-end position for each piRNA were obtained from the bed files using custom R programs.

Analysis of Fem and Masc piRNAs

Each piRNA library was mapped to sequences of *Fem* RNA and *Masc* mRNA (Kiuchi et al. 2014) with Bowtie (Langmead et al. 2009) allowing one mismatch. Sam files were converted to bam files by SAMtools (Li et al. 2009b) and then to bed files by BEDTools (Quinlan and Hall 2010). The length and 5′-end position for each piRNA were obtained from the bed files using custom R programs.

Calculation of 1U/10A-strand bias per transposon

1U/10A-strand bias was calculated for 750 transposons with RPM greater than 10 for both the sense and antisense strands in the siGFP#1 library of embryos. For each transposon, the 1U bias and 10A bias for each strand were calculated, and then the strand with superior 1U bias (1U strand) and the strand with superior 10A bias (10A strand) were defined. As a result, 330 transposons had more 1U (but not 10A) piRNAs in the sense strand and 345 transposons had more 1U (but not 10A) piRNAs in the antisense strand. The 1U strand piRNA/10A strand piRNA of each transposon was then calculated for each small RNA library, and the *z*-scores were calculated by the scale function of R. The "fields" package of R was used to plot the heatmaps.

Calculation of ping-pong Z-score

The calculation of Z-score was based on a previous study (Zhang et al. 2011), with some modifications. The ping-pong Z-score is the difference between the mean of the scores for each overlap from nucleotides 1 to 21 divided by the standard deviation of the background distance scores, defined as the distances 1–9 and 11–21. The calculation of the Z-scores was performed separately for 1U (but not 10A) piRNAs and 10A (but not 1U) piRNAs on the sense strands of transposons.

Prediction of the Gtsf-PIWI/AGO complexes

Protein structures were predicted using AlphaFold ver. 2.1.2 (Evans et al. 2021; Jumper et al. 2021) installed on a local computer via Docker, CUDA Toolkit 11.1. full_dbs was used as a database, and max_template_date was defined as 2021-07-14. Two

protein sequences and a multimer model were used to predict protein complexes (Evans et al. 2021). The heatmaps of predicted aligned errors were made using the pae2png.py script (https://github.com/CYP152N1/plddt2csv). Visualization of the predicted structure was done using PyMOL.

DATA DEPOSITION

The sequencing data is deposited at the DDBJ database (https://www.ddbj.nig.ac.jp) under accession number DRA014298.

SUPPLEMENTAL MATERIAL

Supplemental material is available for this article.

ACKNOWLEDGMENTS

Illumina sequencing was performed in the Vincent J. Coates Genomics Sequencing Laboratory at UC Berkeley, supported by National Institutes of Health (NIH) S10 OD018174 Instrumentation Grant. We thank Phillip Zamore and all the members of the Tomari laboratory for critical comments on the manuscript. This work was in part supported by a Grant-in-Aid for Scientific Research (S) (grant 18H05271 to Y.T.), and Grant-in-Aid for Scientific Research on Innovative Areas (grant 17H06431 to S.K. and T.K.), Grant-in-Aid for Scientific Research (C) (grant 19K06484 to N.I.), and Grant-in-Aid for Early-Career Scientists (grant 22K15082 to K.S.).

Received July 25, 2022; accepted October 19, 2022.

REFERENCES

Anzelon TA, Chowdhury S, Hughes SM, Xiao Y, Lander GC, MacRae IJ. 2021. Structural basis for piRNA targeting. *Nature* **597:** 285–289. doi:10.1038/s41586-021-03856-x

Aravin AA, Van Der Heijden GW, Castañeda J, Vagin VV, Hannon GJ, Bortvin A. 2009. Cytoplasmic compartmentalization of the fetal piRNA pathway in mice. *PLoS Genet* **5:** e1000764. doi:10.1371/journal.pgen.1000764

Arif A, Bailey S, Izumi N, Anzelon TA, Ozata DM, Andersson C, Gainetdinov I, MacRae IJ, Tomari Y, Zamore PD. 2022. GTSF1 accelerates target RNA cleavage by PIWI-clade Argonaute proteins. *Nature* **608:** 618–625. doi:10.1038/s41586-022-05009-0

Brennecke J, Aravin AA, Stark A, Dus M, Kellis M, Sachidanandam R, Hannon GJ. 2007. Discrete small RNA-generating loci as master regulators of transposon activity in *Drosophila*. *Cell* **128:** 1089–1103. doi:10.1016/j.cell.2007.01.043

Chen K, Yu Y, Yang D, Yang X, Tang L, Liu Y, Luo X, Walter J R, Liu Z, Xu J, et al. 2020. *Gtsf1* is essential for proper female sex determination and transposon silencing in the silkworm, *Bombyx mori*. *PLoS Genet* **16:** e1009194. doi:10.1371/journal.pgen.1009194

Chung PY, Shoji K, Izumi N, Tomari Y. 2021. Dynamic subcellular compartmentalization ensures fidelity of piRNA biogenesis in silkworms. *EMBO Rep* **22:** e51342. doi:10.15252/embr.202051342

De Fazio S, Bartonicek N, Di Giacomo M, Abreu-Goodger C, Sankar A, Funaya C, Antony C, Moreira PN, Enright AJ, O'Carroll D. 2011. The endonuclease activity of Mili fuels piRNA amplification that silences LINE1 elements. *Nature* **480:** 259–263. doi:10.1038/nature10547

Ding D, Liu J, Dong K, Midic U, Hess RA, Xie H, Demireva EY, Chen C. 2017. PNLDC1 is essential for piRNA 3′ end trimming and transposon silencing during spermatogenesis in mice. *Nat Commun* **8:** 819. doi:10.1038/s41467-017-00854-4

Dönertas D, Sienski G, Brennecke J. 2013. *Drosophila* Gtsf1 is an essential component of the Piwi-mediated transcriptional silencing complex. *Genes Dev* **27:** 1693–1705. doi:10.1101/gad.221150.113

Evans R, O'Neill M, Pritzel A, Antropova N, Senior AW, Green T, Žídek A, Bates R, Blackwell S, Yim J, et al. 2021. Protein complex prediction with AlphaFold-Multimer. *bioRxiv* doi:10.1101/2021.10.04.463034

Fu Y, Wu P-H, Beane T, Zamore PD, Weng Z. 2018. Elimination of PCR duplicates in RNA-seq and small RNA-seq using unique molecular identifiers. *BMC Genomics* **19:** 531. doi:10.1186/s12864-018-4933-1

Gainetdinov I, Colpan C, Arif A, Cecchini K, Zamore PD. 2018. A single mechanism of biogenesis, initiated and directed by PIWI proteins, explains piRNA production in most animals. *Mol Cell* **71:** 775–790. doi:10.1016/j.molcel.2018.08.007

Ge DT, Wang W, Tipping C, Gainetdinov I, Weng Z, Zamore PD. 2019. The RNA-binding ATPase, Armitage, couples piRNA amplification in Nuage to phased piRNA production on mitochondria. *Mol Cell* **74:** 982–995. doi:10.1016/j.molcel.2019.04.006

Gunawardane LS, Saito K, Nishida KM, Miyoshi K, Kawamura Y, Nagami T, Siomi H, Siomi MC. 2007. A slicer-mediated mechanism for repeat-associated siRNA 5′ end formation in *Drosophila*. *Science* **315:** 1587–1590. doi:10.1126/science.1140494

Haley B, Tang G, Zamore PD. 2003. In vitro analysis of RNA interference in *Drosophila melanogaster*. *Methods* **30:** 330–336. doi:10.1016/s1046-2023(03)00052-5

Han BW, Wang W, Li C, Weng Z, Zamore PD. 2015. piRNA-guided transposon cleavage initiates Zucchini-dependent, phased piRNA production. *Science* **348:** 817–821. doi:10.1126/science.aaa1264

Hayashi R, Schnabl J, Handler D, Mohn F, Ameres SL, Brennecke J. 2016. Genetic and mechanistic diversity of piRNA 3′-end formation. *Nature* **539:** 588–592. doi:10.1038/nature20162

Horwich MD, Li C, Matranga C, Vagin V, Farley G, Wang P, Zamore PD. 2007. The *Drosophila* RNA methyltransferase, DmHen1, modifies germline piRNAs and single-stranded siRNAs in RISC. *Curr Biol* **17:** 1265–1272. doi:10.1016/j.cub.2007.06.030

Ipsaro JJ, Joshua-Tor L. 2022. Developmental roles and molecular mechanisms of Asterix/GTSF1. *Wiley Interdiscip Rev RNA* **13:** e1716. doi:10.1002/wrna.1716

Ipsaro JJ, O'Brien PA, Bhattacharya S, PalmerIII AG, Joshua-Tor L. 2021. Asterix/Gtsf1 links tRNAs and piRNA silencing of retrotransposons. *Cell Rep* **34:** 108914. doi:10.1016/j.celrep.2021.108914

Iwasaki YW, Siomi MC, Siomi H. 2015. PIWI-interacting RNA: its biogenesis and functions. *Annu Rev Biochem* **84:** 405–433. doi:10.1146/annurev-biochem-060614-034258

Izumi N, Shoji K, Sakaguchi Y, Honda S, Kirino Y, Suzuki T, Katsuma S, Tomari Y. 2016. Identification and functional analysis of the pre-piRNA 3′ trimmer in silkworms. *Cell* **164:** 962–973. doi:10.1016/j.cell.2016.01.008

Izumi N, Shoji K, Suzuki Y, Katsuma S, Tomari Y. 2020. Zucchini consensus motifs determine the mechanism of pre-piRNA production. *Nature* **578:** 311–316. doi:10.1038/s41586-020-1966-9

Jumper J, Evans R, Pritzel A, Green T, Figurnov M, Ronneberger O, Tunyasuvunakool K, Bates R, Žídek A, Potapenko A, et al. 2021. Highly accurate protein structure prediction with AlphaFold. *Nature* **596:** 583–589. doi:10.1038/s41586-021-03819-2

Kawaoka S, Hayashi N, Suzuki Y, Abe H, Sugano S, Tomari Y, Shimada T, Katsuma S. 2009. The *Bombyx* ovary-derived cell line endogenously expresses PIWI/PIWI-interacting RNA complexes. *RNA* **15:** 1258–1264. doi:10.1261/rna.1452209

Kawaoka S, Arai Y, Kadota K, Suzuki Y, Hara K, Sugano S, Shimizu K, Tomari Y, Shimada T, Katsuma S. 2011. Zygotic amplification of secondary piRNAs during silkworm embryogenesis. *RNA* **17:** 1401–1407. doi:10.1261/rna.2709411

Kirino Y, Mourelatos Z. 2007. The mouse homolog of HEN1 is a potential methylase for Piwi-interacting RNAs. *RNA* **13:** 1397–1401. doi:10.1261/rna.659307

Kiuchi T, Katsuma S. 2022. Functional characterization of silkworm PIWI proteins by embryonic RNAi. *Methods Mol Biol* **2360:** 19–31. doi:10.1007/978-1-0716-1633-8_3

Kiuchi T, Koga H, Kawamoto M, Shoji K, Sakai H, Arai Y, Ishihara G, Kawaoka S, Sugano S, Shimada T, et al. 2014. A single female-specific piRNA is the primary determiner of sex in the silkworm. *Nature* **509:** 633–636. doi:10.1038/nature13315

Langmead B, Trapnell C, Pop M, Salzberg SL. 2009. Ultrafast and memory-efficient alignment of short DNA sequences to the human genome. *Genome Biol* **10:** R25. doi:10.1186/gb-2009-10-3-r25

Li C, Vagin VV, Lee S, Xu J, Ma S, Xi H, Seitz H, Horwich MD, Syrzycka M, Honda BM, et al. 2009a. Collapse of germline piRNAs in the absence of Argonaute3 reveals somatic piRNAs in flies. *Cell* **137:** 509–521. doi:10.1016/j.cell.2009.04.027

Li H, Handsaker B, Wysoker A, Fennell T, Ruan J, Homer N, Marth G, Abecasis G, Durbin R. 2009b. The sequence alignment/map format and SAMtools. *Bioinformatics* **25:** 2078–2079. doi:10.1093/bioinformatics/btp352

Martin M. 2011. Cutadapt removes adapter sequences from high-throughput sequencing reads. *EMBnet J* **17:** 10–12. doi:10.14806/ej.17.1.200

Mohn F, Handler D, Brennecke J. 2015. piRNA-guided slicing specifies transcripts for Zucchini-dependent, phased piRNA biogenesis. *Science* **348:** 812–817. doi:10.1126/science.aaa1039

Muerdter F, Guzzardo PM, Gillis J, Luo Y, Yu Y, Chen C, Fekete R, Hannon GJ. 2013. A genome-wide RNAi screen draws a genetic framework for transposon control and primary piRNA biogenesis in *Drosophila*. *Mol Cell* **50:** 736–748. doi:10.1016/j.molcel.2013.04.006

Nishida KM, Iwasaki YW, Murota Y, Nagao A, Mannen T, Kato Y, Siomi H, Siomi MC. 2015. Respective functions of two distinct Siwi complexes assembled during PIWI-interacting RNA biogenesis in *Bombyx* germ cells. *Cell Rep* **10:** 193–203. doi:10.1016/j.celrep.2014.12.013

Nishida KM, Sakakibara K, Sumiyoshi T, Yamazaki H, Mannen T, Kawamura T, Kodama T, Siomi MC. 2020. Siwi levels reversibly regulate secondary pi RISC biogenesis by affecting Ago3 body morphology in *Bombyx mori*. *EMBO J* **39:** e105130. doi:10.15252/embj.2020105130

Nishimura T, Nagamori I, Nakatani T, Izumi N, Tomari Y, Kuramochi-Miyagawa S, Nakano T. 2018. PNLDC 1, mouse pre-pi RNA Trimmer, is required for meiotic and post-meiotic male germ cell development. *EMBO Rep* **19:** e44957. doi:10.15252/embr.201744957

Ohtani H, Iwasaki YW, Shibuya A, Siomi H, Siomi MC, Saito K. 2013. DmGTSF1 is necessary for Piwi–piRISC-mediated transcriptional transposon silencing in the *Drosophila* ovary. *Genes Dev* **27:** 1656–1661. doi:10.1101/gad.221515.113

Osanai-Futahashi M, Suetsugu Y, Mita K, Fujiwara H. 2008. Genome-wide screening and characterization of transposable elements and their distribution analysis in the silkworm, *Bombyx mori*. *Insect Biochem Mol Biol* **38:** 1046–1057. doi:10.1016/j.ibmb.2008.05.012

Ozata DM, Gainetdinov I, Zoch A, O'Carroll D, Zamore PD. 2019. PIWI-interacting RNAs: small RNAs with big functions. *Nat Rev Genet* **20:** 89–108. doi:10.1038/s41576-018-0073-3

Quinlan AR, Hall IM. 2010. BEDTools: a flexible suite of utilities for comparing genomic features. *Bioinformatics* **26:** 841–842. doi:10.1093/bioinformatics/btq033

Reuter M, Berninger P, Chuma S, Shah H, Hosokawa M, Funaya C, Antony C, Sachidanandam R, Pillai RS. 2011. Miwi catalysis is required for piRNA amplification-independent LINE1 transposon silencing. *Nature* **480:** 264–267. doi:10.1038/nature10672

Saito K, Sakaguchi Y, Suzuki T, Suzuki T, Siomi H, Siomi MC. 2007. Pimet, the *Drosophila* homolog of HEN1, mediates 2′-*O*-methylation of Piwi-interacting RNAs at their 3′ ends. *Genes Dev* **21:** 1603–1608. doi:10.1101/gad.1563607

Takemoto N, Yoshimura T, Miyazaki S, Tashiro F, Miyazaki J. 2016. *Gtsf1l* and *Gtsf2* are specifically expressed in gonocytes and spermatids but are not essential for spermatogenesis. *PLoS ONE* **11:** e0150390. doi:10.1371/journal.pone.0150390

Wang W, Yoshikawa M, Han BW, Izumi N, Tomari Y, Weng Z, Zamore PD. 2014. The initial uridine of primary piRNAs does not create the tenth adenine that Is the hallmark of secondary piRNAs. *Mol Cell* **56:** 708–716. doi:10.1016/j.molcel.2014.10.016

Williams Z, Ben-Dov IZ, Elias R, Mihailovic A, Brown M, Rosenwaks Z, Tuschl T. 2013. Comprehensive profiling of circulating microRNA via small RNA sequencing of cDNA libraries reveals biomarker potential and limitations. *Proc Natl Acad Sci* **110:** 4255–4260. doi:10.1073/pnas.1214046110

Yoda M, Kawamata T, Paroo Z, Ye X, Iwasaki S, Liu Q, Tomari Y. 2010. ATP-dependent human RISC assembly pathways. *Nat Struct Mol Biol* **17:** 17–23. doi:10.1038/nsmb.1733

Yoshimura T, Toyoda S, Kuramochi-Miyagawa S, Miyazaki T, Miyazaki S, Tashiro F, Yamato E, Nakano T, Miyazaki J. 2009. *Gtsf1/Cue110*, a gene encoding a protein with two copies of a CHHC Zn-finger motif, is involved in spermatogenesis and retrotransposon suppression in murine testes. *Dev Biol* **335:** 216–227. doi:10.1016/j.ydbio.2009.09.003

Yoshimura T, Watanabe T, Kuramochi-Miyagawa S, Takemoto N, Shiromoto Y, Kudo A, Kanai-Azuma M, Tashiro F, Miyazaki S, Katanaya A, et al. 2018. Mouse GTSF 1 is an essential factor for secondary piRNA biogenesis. *EMBO Rep* **19:** e42054. doi:10.15252/embr.201642054

Zhang Z, Xu J, Koppetsch BS, Wang J, Tipping C, Ma S, Weng Z, Theurkauf WE, Zamore PD. 2011. Heterotypic piRNA Ping-Pong requires Qin, a protein with both E3 ligase and Tudor domains. *Mol Cell* **44:** 572–584. doi:10.1016/j.molcel.2011.10.011

Zhang Y, Guo R, Cui Y, Zhu Z, Zhang Y, Wu H, Zheng B, Yue Q, Bai S, Zeng W, et al. 2017. An essential role for PNLDC1 in piRNA 3′ end trimming and male fertility in mice. *Cell Res* **27:** 1392–1396. doi:10.1038/cr.2017.125

See the following page for ***Meet the First Author***

MEET THE FIRST AUTHOR

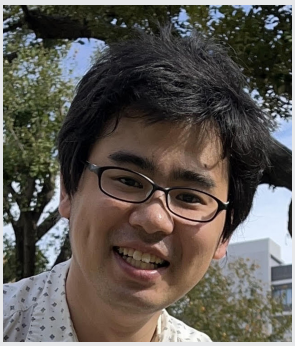

Keisuke Shoji

***Meet the First Author(s)* is a new editorial feature within *RNA*, in which the first author(s) of research-based papers in each issue have the opportunity to introduce themselves and their work to readers of *RNA* and the RNA research community. Natsuko Izumi and Keisuke Shoji are first authors of this paper, "The two Gtsf paralogs in silkworms orthogonally activate their partner PIWI proteins for target cleavage." Natsuko is a technical specialist and Keisuke is a Research Associate in Dr. Yukihide Tomari's laboratory at the University of Tokyo, specializing in biochemical experiments and bioinformatics analysis, respectively.**

What are the major results described in your paper and how do they impact this branch of the field?

piRNAs play a vital role in protecting the germline genome from transposons. Endonucleolytic cleavage of piRNA-complementary target RNAs by PIWI proteins is one of the central strategies for transposon silencing. The PIWI-catalyzed target cleavage is also coupled with synthesis of new piRNAs. Therefore, the catalytic activity of PIWI protein is crucial in the piRNA pathway.

Previous studies have shown that Gametocyte-specific factor 1 (Gtsf1), a small zinc finger protein, is an essential factor for the piRNA pathway. Recently, we and our collaborators have discovered that mouse GTSF1 greatly accelerates the otherwise weak catalytic activity of MILI and MIWI, and proposed that this PIWI-potentiating role of the Gtsf1 protein family may be widely conserved.

In this study, we systematically and carefully dissected the function of silkworm Gtsf1 and its paralog Gtsf1-like (Gtsf1L) in the piRNA pathway. We found that Gtsf1 and Gtsf1L preferentially interact with the two silkworm PIWI proteins Siwi and BmAgo3, respectively, and promote the catalytic activity of each PIWI protein. This paper is expected to improve our understanding of how the piRNA pathway is optimized for each organism and what happens when PIWI proteins function.

What led you to study RNA or this aspect of RNA science?

KS: In a recent paper, Dr. Izumi analyzed the function of Gtsf in mice and silkworm. Thus, we decided to take a closer look at Gtsf in the silkworm, which we usually study. Many animals possess multiple Gtsf paralogs; flies have four, mice have three, and silkworms have two. Therefore, we aimed to analyze the function of Gtsf in the silkworm, and to determine part of the reason as to why they have multiple Gtsfs.

During the course of these experiments, were there any surprising results or particular difficulties that altered your thinking and subsequent focus?

KS: There are two silkworm Gtsfs and two PIWI proteins each, with Gtsf1 interacting with Siwi and Gtsf1L with BmAgo3. However, small RNA analysis showed that Gtsf1 depletion affected the piRNA of BmAgo3, while Gtsf1L deficiency affected the piRNA of Siwi. I was initially surprised that the interaction and the affected piRNAs were different.

What are some of the landmark moments that provoked your interest in science or your development as a scientist?

KS: Perhaps one of the moments is the experience of having my mother read me *Fabre's Book of Insects* when I was young. I have a one-year-old daughter and would like to read to her soon.

If you were able to give one piece of advice to your younger self, what would that be?

KS: You will sit in front of the computer all the time, and won't exercise, so don't eat too many snacks!

What were the strongest aspects of your collaboration as co-first authors?

KS: I perform the bioinformatics analysis and Dr. Izumi performs the extraordinary biochemical analysis. We complement each other well, with biochemical analysis showing solid results, and bioinformatics showing overall trends and hypotheses derived from them.